The Astrophysical Journal Supplement Series, 216:26 (13pp), 2015 February doi:10.1088/0067-0049/216/2/26

A *GALEX*-BASED SEARCH FOR THE SPARSE YOUNG STELLAR POPULATION IN THE TAURUS–AURIGAE STAR FORMING REGION

Ana I. Gómez de Castro[1], Javier Lopez-Santiago[1], Fatima López-Martínez[1], Néstor Sánchez[1], Paola Sestito[1], Elisa de Castro[2], Manuel Cornide[2], and Javier Yañez Gestoso[1]
[1] AEGORA Research Group, Universidad Complutense de Madrid, Plaza de Ciencias 3, E-28040 Madrid, Spain
[2] Fac. de CC. Físicas, Universidad Complutense de Madrid, Plaza de Ciencias 1, E-28040 Madrid, Spain
Received 2013 October 26; accepted 2014 December 3; published 2015 January 27

ABSTRACT

In this work, we identify 63 bona fide new candidates to T Tauri stars (TTSs) in the Taurus–Auriga region, using its ultraviolet excess as our baseline. The initial data set was defined from the *GALEX* all sky survey (AIS). The *GALEX* satellite obtained images in the near-ultraviolet (NUV) and far-ultraviolet (FUV) bands where TTSs show a prominent excess compared with main-sequence or giants stars. *GALEX* AIS surveyed the Taurus–Auriga molecular complex, as well as a fraction of the California Nebula and the Perseus complex; bright sources and dark clouds were avoided. The properties of TTSs in the ultraviolet (*GALEX*), optical (UCAC4), and infrared (2MASS) have been defined using the TTSs observed with the International Ultraviolet Explorer reference sample. The candidates were identified by means of a mixed ultraviolet-optical-infrared excess set of colors; we found that the FUV–NUV versus $J-K$ color–color diagram is ideally suited for this purpose. From an initial sample of 163,313 bona fide NUV sources, a final list of 63 new candidates to TTSs in the region was produced. The search procedure has been validated by its ability to detect all known TTSs in the area surveyed: 31 TTSs. Also, we show that the weak-lined TTSs are located in a well-defined stripe in the FUV–NUV versus $J-K$ diagram. Moreover, in this work, we provide a list of TTSs photometric standards for future *GALEX*-based studies of the young stellar population in star forming regions.

Key words: Galaxy: stellar content – stars: variables: T Tauri, Herbig Ae/Be – surveys – ultraviolet: stars

Supporting material: machine-readable table

1. INTRODUCTION

T Tauri stars (TTSs) are precursors to solar-like stars and planetary systems. As such, their study is fundamental for our comprehension of the solar system's formation, evolution, and planetary build up. Around the location of Earth in the Galaxy, there is a ring of star forming regions that constitutes the main laboratory for the study of the early phases of solar system formation. Regions like Taurus, Aurigae, Lupus, Chamaleon, or Ophiuchus are within a radius of 140 pc around the Earth, in a clean area of the Galaxy where extinction is low. Moreover, they are at low galactic latitudes ($-20^\circ < b_{\rm gal} < 20^\circ$), minimizing the pollution of UV surveys from background galaxies. These regions form mainly solar-like stars (though B stars are observed in Ophiuchus and A stars in Aurigae). All together, they cover a large area of the sky, with the Taurus–Auriga complex being the most extended, roughly 20 × 20 square degrees in the sky.

The identification of TTSs in these regions has proceeded at a fast rate: from the first observations of infrared excess and magnetically active stars in the neighborhood of the molecular clouds (see, i.e., Strom et al. 1976; Herbig & Bell 1988; Lada 1983) to the late use of large-scale surveys of the Galaxy (Neuhaeuser et al. 1995; Wichmann et al. 1996; Li & Hu 1998; Kohoutek & Wehmeyer 1999; Rebull et al. 2011; Esplin et al. 2014). In all of these works, lists of candidates have been compiled. To search for candidates, these investigations resorted to some basic properties of the TTSs, such as their proximity to the molecular clouds, the equivalent width of the Hα line, their proper motions and kinematics, or their enhanced X-ray flux. For the final source identification, authors usually resort to the optical to infrared spectral energy distribution (SED) for CTTSs; the accretion disk imprint is clearly apparent in the SED. However, for WTTSs, spectroscopic follow-up observations are adopted as the most reliable means of source identification; in particular, the strength of Li I absorption is a reliable tracer of youth (see, i.e., Wichmann et al. 1996).

The search for candidates requires that we understand the distinct nature of the TTSs with respect to other galactic sources. TTSs display excess emission in various wavelength ranges compared with their main-sequence analogs. This excess is caused by the release of gravitational energy during the star formation process. The conservation of angular momentum during gravitational collapse drives the formation of accretion disks that channel the infall of matter onto the star. Disks become heated by the dissipation of the angular momentum excess to small scales through the action of magnetorotational instability, according to the current paradigm. The magnetically mediated interaction between the slowly rotating pre-main-sequence (PMS) star and the disk drives the production of jets and outflows (see Gómez de Castro 2013a for a recent review). As a result, TTSs display the following:

1. an infrared to millimeter wavelengths excess caused either directly by the disk radiative output itself or through disk reprocessing of the stellar and jet radiation (see, for instance, early works such as Mendoza & Eugenio 1968 or recent works such as Furlan et al. 2011 or Jensen et al. 2009);
2. an optical excess caused by the veiling continuum produced by plasma at a nominal temperature of about 7000–10,000 K that represents the low-energy tail of the ultraviolet (UV) spectrum (see, for instance, early works such as Basri & Batalha 1990 or the recent works by Ingleby et al. 2013);

3. an ultraviolet (UV) excess produced by plasma with electron temperatures ranging from 10,000 K–50,000 K that appears as both a warm continuum and a distinct set of spectral indicators; excess emission is observed in neutral species (H I, O I, C I), singly ionized species (C II, Si II, Fe II, Mg II, O II), and all the way to highly ionized species such as C IV, N V, or O VI, not to mention the H_2 molecular emission in the Werner bands. This excess is produced by the sheared magnetosphere-disk boundary layer and the magnetospheric accretion flow with a non-negligible contribution from the outflow and the inner disk (see Gómez de Castro 2009 for a detailed review on the UV spectrum of the TTSs);
4. an X-ray excess (see, for instance, from early works by Montmerle et al. 1983 and reviews such as Preibisch 2004) produced by the strong magnetospheric activity, the expanded corona, and the accretion shocks at the point of impact where the gravitational energy of the infalling material is finally released in heating(i.e., Lamzin 1998; Calvet & Gullbring 1998).

Despite the relevance of the UV excess of TTSs compared to that of their main-sequence analogs, most searches for candidates have been run at either X-ray (see, for instance, Feigelson et al. 2005; Neuhaeuser et al. 1995) or infrared wavelengths (Furlan et al. 2011; Takita et al. 2010; Padgett et al. 2006). Only the southern area of the Taurus complex was surveyed to search for TTSs in the UV (Findeisen & Hillenbrand 2010; hereafter FH). The release of the *GALEX* All Sky Survey (hereafter *GALEX*/AIS) has provided an amazing wealth of information on the UV characteristics of the galactic stellar population (Bianchi et al. 2014) in general, and of Gould's Belt or the local supercomplex of star formation (Gómez de Castro et al. 2011) in particular. Among all of the possible regions of star formation, the Taurus–Auriga complex is the prototype for low-mass star formation and is the best studied (Kenyon et al. 2008). The complex contains many dark nebulae, Herbig–Haro jets and outflows, and young stars. With few massive O or B stars, the clouds are an excellent place to study the formation of Sun-like stars, in contrast with the Orion Nebula Cluster, at 450 pc, where a significant population of young massive stars resides.

The *GALEX*/AIS survey of the Taurus–Auriga molecular complex consists of 197 *GALEX* fields covering 380 square degrees in the sky; more than three times larger than the FH survey. About 163,000 NUV sources have been detected, allowing for detailed studies of the stellar population in this area of the Galaxy as well as searches for young stars. The area mapped by *GALEX* also includes the northern tip (in galactic coordinates) of the Hyades stellar association.

In this work, we have developed a set of new criteria, different from those proposed by FH, to search for TTSs in UV surveys. Our method makes use of the known spectral energy distribution of TTSs in the UV to derive the UV magnitudes of the TTSs in the *GALEX* bands. Once we validated this method, we used a combination of UV and IR colors to discriminate TTSs from the background stellar population.

Our working sample consists of 163,313 UV sources that have been cross-correlated with optical and IR catalogs to produce a number of color–color and color–magnitude diagrams. From that sample, a total of 63 new candidate TTSs have been found. In Section 2, we calculate the photometric properties of TTSs in the *GALEX* bands. In Section 3, we outline the main characteristics of the *GALEX* survey; the multi-band photometric criteria are defined and applied to the *GALEX* sample to produce a preliminary list of candidates. In the process, 31 known TTSs within the area mapped by *GALEX*-AIS are retrieved. As a result, a more robust database is established to qualify TTSs candidates in the *GALEX* AIS survey. This data base is used in Section 4 to further refine the search and produce a final list of 63 new candidates, most of them class II-III sources (Wilking & Lada 1983). A short discussion about the location of the new TTS candidates in the TMC and a brief summary are provided in Sections 5 and 6, respectively.

2. PROPERTIES OF THE TTSs IN THE *GALEX* BANDS

GALEX was a 50 cm primary space telescope with a Ritchey–Chretien mounting simultaneously feeding two detectors sensitive to near- and far-UV using a multilayer dichroic beamsplitter. The near-UV (NUV) channel works in the 1770–2730 Å spectral range and the far-UV (FUV) channel in the 1350–1780 Å range; the transmittance curves of the channels are shown in Figure 1, together with the UV spectrum of T Tau, the prototype of TTS. The characteristics of the plasma sampled by the NUV and FUV bands are quite distinct.

1. The spectrum of TTSs in the FUV band contains mainly emission lines covering a very broad range of plasma temperatures: from the molecular bands of H_2 (Herczeg et al. 2002; France et al. 2011) to the resonance transitions of Si IV, C IV, C I, and He II (Gómez de Castro & Franqueira 1997; Valenti et al. 2000; Yang et al. 2012; Gómez de Castro & Marcos-Arenal 2012; Ardila et al. 2013; Gómez de Castro 2013b). The peak of the band is at 1500 Å and hence *GALEX* FUV band radiation is dominated by the fluorescence H_2 radiation and the C IV, He II, and Si IV features. Radiation in these lines correlates with the accretion rate (see, France et al. 2012; Ardila et al. 2013; Gómez de Castro 2013, for the most recent references in the field). In cool stars, radiation in the *GALEX* FUV band correlates with the stellar activity, as measured by the H, K, Ca II index (Findeisen et al. 2011).
2. The spectrum of TTSs in the NUV band mainly contains radiation from warm plasma at temperatures between 3000 K and some 10,000 K: the dominant features being the Mg II[uv1] multiplet, the Fe II resonance multiplets [uv1], [uv2], and [uv3], the C II] feature at 2326 Å and the short wavelength tail of the Balmer continuum. The transmittance curve of the band enhances the radiation from the Fe II multiplets and the 2326 Å feature with respect to Mg II radiation, the strongest line in the NUV spectrum. For instance, in T Tau, 38% of the NUV radiation is in the $\mathrm{C\,II]_{2323}}$, Mg II, and Fe II lines. Both the line radiation and continuum correlate with the accretion rate and chromospheric activity.

These trends are readily shown in Figures 2 and 3. In Figure 2, the C IV line excess radiation in TTSs is compared with that of main-sequence cool stars, including very active M-dwarfs (from Gómez de Castro & Marcos-Arenal 2012). As is shown, TTSs are several orders of magnitude brighter, allowing us to detect them at the 140 pc distance of TMC. Therefore, radiation in the FUV band can be used as reliably as Hα or X-ray radiation surveys to identify TTSs by their unusual strength. In Figure 3, the M_V versus UV-V color is plotted for simultaneous near-UV and optical observations obtained with *IUE* of TTSs (Gomez de Castro 1997). The locations of the late-type (K3 or later) TTSs in the diagram are plotted against the locations of cool main-sequence stars. A quick inspection shows that the UV–V color

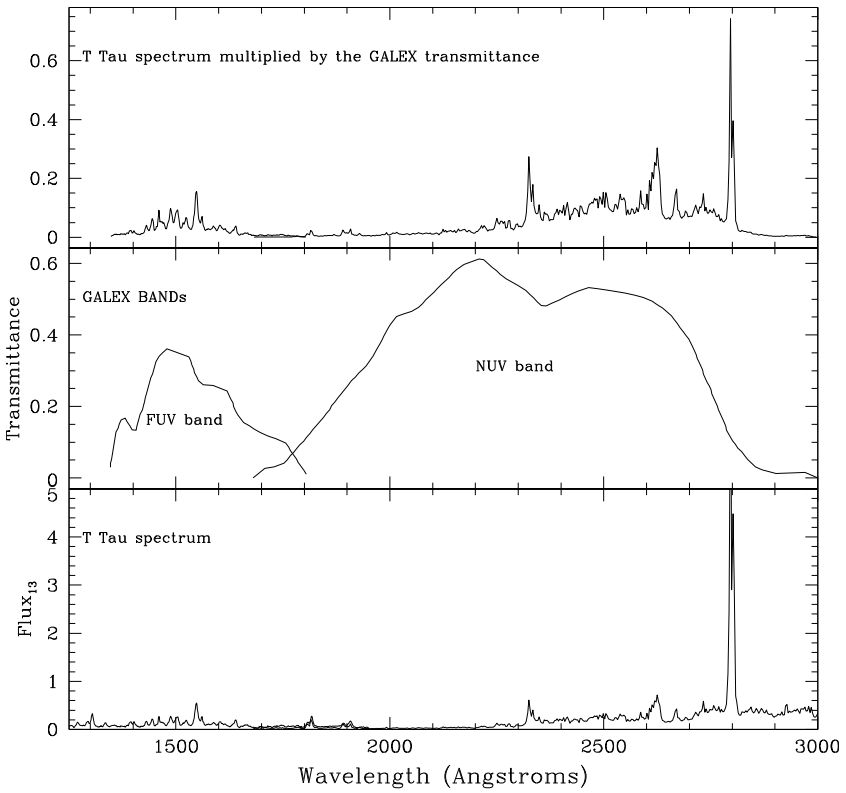

Figure 1. T Tau spectrum (bottom), *GALEX* FUV and NUV channels spectral response (middle), and T Tau spectrum multiplied by the *GALEX* spectral response. The stellar flux in the bottom panel is given in units of 10^{-13} erg cm^{-2} s^{-1} Å^{-1}.

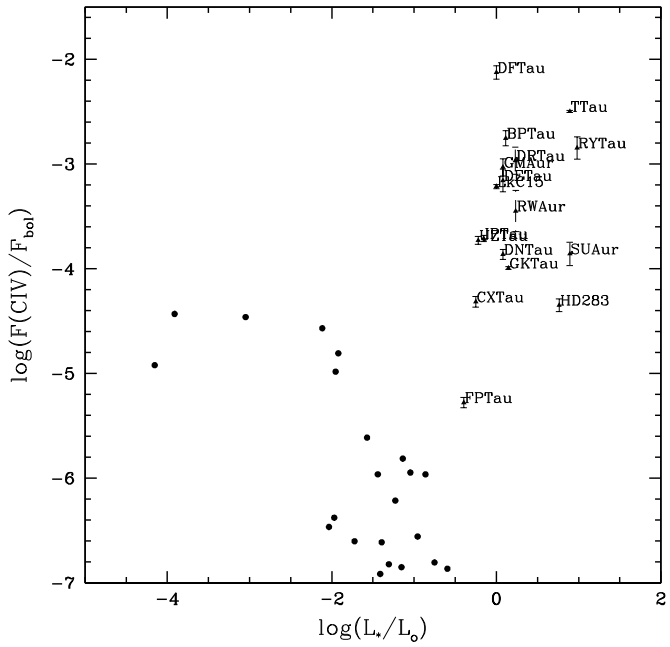

Figure 2. Some characteristics of the UV excess in the TTSs. (UV-V, V) color – magnitude diagram for the T Tauri stars observed with the *IUE* in the Taurus region. The crosses represent cool TTSs (spectral types later than ∼ K3) and the open circles warm TTSs (spectral types earlier than ∼ K3). The location of the main sequence is also marked from *IUE* observations. The TTSs closer to the main sequence are the WTTSs (from Gomez de Castro 1997).

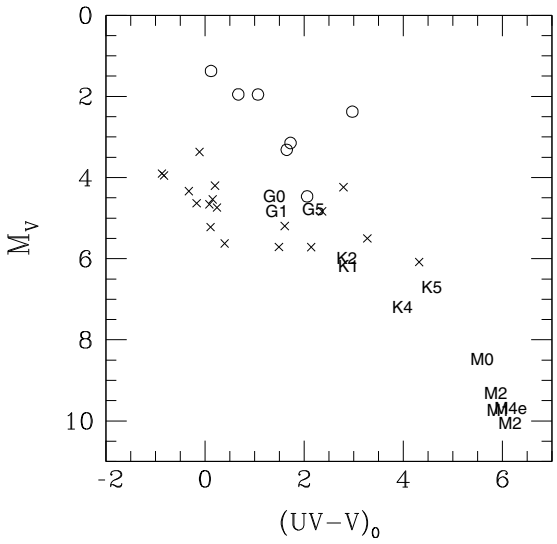

Figure 3. Some characteristics of the UV excess in the TTSs. The normalized fluxes are represented vs. the stellar luminosities for the C IV line (similar relations are observed for other spectral tracers in the FUV band; see Gómez de Castro & Marcos-Arenal 2012). TTSs and main-sequence cool stars are plotted with triangles and circles, respectively. Me stars are found to be as strong in the UV as WTTSs. Error bars for the UV-normalized fluxes of the TTSs are indicated.

decreases as the TTSs approach the main sequence, but that the color excess is negligible in Weak-lined TTSs (WTTSs).

To derive the expected photometric properties of the TTSs in the *GALEX* bands, we have used the sample of the TTSs observed with the *IUE* in low dispersion mode and compiled by Gómez de Castro & Franqueira 1997 for the *IUE* Uniform Low Dispersion Archive Guides (hereafter GdCF); only the 21 TTSs with high signal-to-noise ratio spectra over the whole range were selected for this purpose (see Table 1). Their *IUE* spectra have been multiplied by the normalized *GALEX* transmittance function in the FUV and NUV windows to compute their FUV

Table 1
T Tauri Stars used as Reference Sample[a,b]

HBC	Star	Spectral[c] Type	d (pc)	FUV (AB mag)	NUV (AB mag)	R (mag)	J (mag)	H (mag)	K (mag)
10	WY Ari	K5 Bin	275	17.36	15.26	12.4	10.229 ± 0.021	9.418 ± 0.021	8.901 ± 0.018
32	BP Tau	K7	140	17.66	15.97	11.62	9.098 ± 0.037	8.220 ± 0.024	7.736 ± 0.023
33	DE Tau	M2	140	17.96	16.49	11.93	9.180 ± 0.022	8.273 ± 0.018	7.799 ± 0.018
34	RY Tau	K1	140	17.73	15.38	9.67	7.155 ± 0.019	6.13 ± 0.06	5.395 ± 0.023
35	T Tau	K0	140	16.42	14.97	9.8	7.240 ± 0.023	6.237 ± 0.017	5.325 ± 0.017
36	DF Tau	M0-1	140	17.58	16.78	11.50	8.171 ± 0.026	7.256 ± 0.023	6.734 ± 0.024
74	DR Tau	K4	140	16.95	14.87	12.19 ± 0.41	8.845 ± 0.024	7.80 ± 0.05	6.874 ± 0.017
77	GM Aur	K3	140	17.57	16.39	11.22	9.341 ± 0.018	8.603 ± 0.024	8.283 ± 0.017
79	SU Aur	G2	140	18.04	15.21	9.17	7.199 ± 0.020	6.558 ± 0.020	5.990 ± 0.023
80	RW Aur	K1	140	16.51	14.13	9.95	8.378 ± 0.024	7.621 ± 0.038	7.020 ± 0.018
85	GW Ori	G5	450	17.44	15.02	9.52	7.698 ± 0.030	7.103 ± 0.029	6.590 ± 0.029
247	CV Cha	G8	175	17.32	14.94	10.51	8.285 ± 0.023	7.46 ± 0.04	6.845 ± 0.026
251	RU Lup	K7	140	15.85	13.41	9.99	8.732 ± 0.026	7.824 ± 0.042	7.138 ± 0.024
271	AK Sco	F5 SB	145	17.15	14.01	9.2	7.676 ± 0.026	7.06 ± 0.03	6.503 ± 0.020
315	DI Cep	G8	244	17.51	15.11	10.49	9.302 ± 0.026	8.572 ± 0.047	7.952 ± 0.026
380	HD 283572	G5	140	18.75	14.77	9.14	7.414 ± 0.029	7.008 ± 0.026	6.869 ± 0.023
435	AB Dor	K0	15	16.32	12.8	6.496	5.316 ± 0.019	4.845 ± 0.033	4.686 ± 0.016
568	TW Hya	K7	56	15.65	14.00	10.19	8.217 ± 0.024	7.558 ± 0.042	7.297 ± 0.024
656	V2398 Oph	G8	125	16.23	14.48	10.1[d]	8.62 ± 0.024	7.810 ± 0.046	7.23 ± 0.08
662	V4046 Sgr	K5,6 SB	83	16.60	16.05	9.67[e]	8.071 ± 0.023	7.435 ± 0.051	7.249 ± 0.020
664	FK Ser	K7 Bin	350	17.72	16.19	9.41	7.636 ± 0.020	6.92 ± 0.03	6.624 ± 0.021

Notes.
[a] see Gómez de Castro & Franqueira 1997 for more details and R values.
[b] JHK mag from 2MASS.
[c] SB: Spectroscopic Binary.
[d] UCAC4 catalogue, Zacharias et al. 2013.
[e] Hutchinson et al. 1990.

and NUV AB magnitudes using the Morrissey et al. (2007) conversion:

$$\mathrm{NUV} = -2.5 \times \log\left(\frac{\text{Flux NUV}}{2.06 \times 10^{-16}\ \mathrm{erg\ s^{-1}\ cm^{-2}\ \AA^{-1}}}\right) + 20.08$$

$$\mathrm{FUV} = -2.5 \times \log\left(\frac{\text{Flux FUV}}{1.40 \times 10^{-15}\ \mathrm{erg\ s^{-1}\ cm^{-2}\ \AA^{-1}}}\right) + 18.82.$$

This *IUE* sample is scarce in terms of WTTSs and M-type CTTSs due to the sensitivity of the *IUE*. Also note that given the spectral energy distribution of TTSs, their FUV magnitude is rather low (especially for WTTSs), and as a result it is challenging to detect cool WTTSs in the *GALEX* FUV band (see below).

3. THE *GALEX* SURVEY OF THE TMC

The baseline of the *GALEX* All Sky Survey was completed in 2007. *GALEX*/AIS covers 26,000 deg^2 (∼63% of the Sky) and provides broadband imaging in two UV bands. *GALEX* obtained 197 images on the Taurus molecular cloud for a total coverage of ∼200 deg^2 (see Figure 4); note that the *GALEX* field of view is circular with a radius of 0.°6. The *GALEX* mission provides as output products for each tile (or image in the AIS survey) several files containing the pipeline processed images in the FUV and NUV bands, the intermediate calibration files, and the catalog of sources identified in each pointing; the sources in the catalog are identified with the SExtractor procedure (Morrissey et al. 2007) and their FUV and NUV magnitudes are provided. Typically, the number of sources in the catalog outnumber by a factor of two to three the number of sources that can be identified as such from a simple inspection of the images. The detection procedure clearly suffers from overestimation of actual sources. The number of spurious detections is very large.

To overcome this problem, we have designed a strategy that guarantees no TTSs are lost in the cross-identification procedure. TTSs are stars with photospheric spectral types F to M and an infrared excess that decreases as stars approach the main sequence. As an example, in Figure 5, we display the spectral energy distribution of AK Sco located 145 pc from the Sun. The prominent FUV and infrared excesses are readily recognized over the stellar atmosphere radiative output predicted by the Kurucz model of an F5 star (Alencar et al. 2003). Thus, cross-identification with galactic sources from the Fourth USNO CCD Astrograph Catalog - U.S. Naval Observatory (UCAC4; Zacharias et al. 2013) and the 2MASS surveys (Skrutskie et al. 2006) is a reliable means for removing spurious sources without losing TTSs in the procedure.

Bona fide *GALEX* sources were identified as having a 2MASS counterpart within a search radius of 3 arcsec. This search radius was carefully selected after a precise study of the shift between 2MASS and *GALEX* sources in the TMC (see Gómez de Castro et al. 2011, for details). After cross-match, all sources satisfied NUV $\lesssim$ 22 mag, which corresponds to the ∼3σ detection threshold for a typical exposure time of 100 s (Bianchi et al. 2011). The magnitude completeness limits for 2MASS are 15.8, 15.1, and 14.3 mag in the J, H, and K_s bands, respectively. These limits are well above the magnitude of M-type stars at the distance of the Taurus–Auriga molecular complex. The J absolute magnitude for a 4 Myr old M5 star is ∼5.5 (e.g., Siess et al. 2000). At a distance of 140 pc, the magnitude of such a star is $J \sim 11.5$ mag. Even in the case of notable ISM extinction $A_J = 4$ mag, the star would be detected by 2MASS

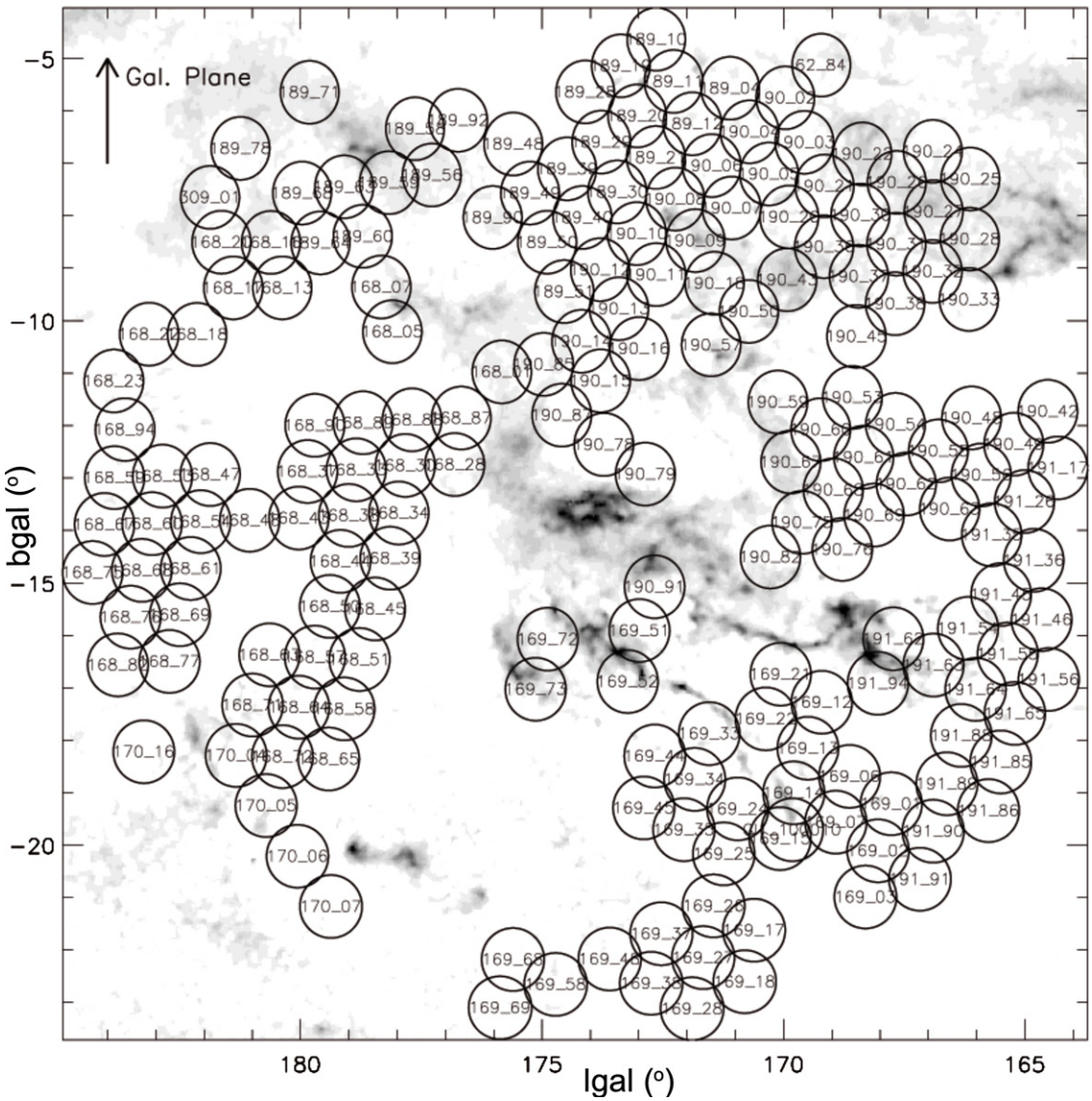

Figure 4. Location and tile identification of the *GALEX* AIS images used in the work. The molecular gas distribution, as unveiled by the 2MASS extinction map (Lombardi et al. 2010), is overlaid for reference.

at the distance of the molecular cloud. Similarly, UCAC4 is complete from the brightest stars to about $R = 16$ mag. This means that UCAC4 is complete for mid-M stars at the distance of the Taurus cloud for extinctions $A_V < 2$ mag. As we do not expect large extinctions for our stars because they were selected from the UV, we can conclude that we are complete for members of the star-forming region for the entire luminosity function, from the more massive to the less massive stars. This does not assure completeness down to M dwarfs at 140 pc (e.g., Lépine & Gaidos 2011).

The *GALEX* AIS survey is, however, deep enough to reach the TTSs population in the TMC. A bright CTTS such as RW Aur, a K3 spectral type with $A_V = 0.5$ mag (Ingleby et al. 2013), is found to have FUV = 15.9 and NUV = 13.8 in the *GALEX* bands, and a WTTS such as V836 Tau (K7) with $A_V = 1.5$ (Ingleby et al. 2013) has FUV = 20.8 and NUV = 19.9. Both stars are 140 pc from the Sun. As shown below, the *GALEX*/AIS limiting magnitude in the very demanding FUV channel is 22.3 for this survey. In summary, the survey must be complete to the TMC distance for CTTSs and most WTTSs, except for embedded sources and very late types. Non-extincted sources as bright as RW Aur could be detected as far away as 2.2 kpc. Otherwise, RW Aur would be detectable even if extincted by $A_V = 2.7$ mag instead of 0.5 mag; the Fitzpatrick (1999) extinction law has been assumed (see Yuan et al. 2013 for a discussion about possible deviations of the ISM extinction law in the NUV and FUV bands).

After cross-correlation, we retained a total of 163,313 UV sources as reliable detections. All them have, at least, a 2MASS counterpart at less than 3 arcsec. Figure 6 shows the density map of our sources in the selected region. The 2MASS extinction map by Lombardi et al. (2010) is overplotted. Spatial binning is 3 arcmin^2 and the color code ranges from 0 to 8 sources per arcminute. The stellar density is clearly not homogeneous. Many regions suffer from large extinction, coinciding with the location of dense molecular clouds. However, the density of UV stars is also low in some regions where extinction is low as inferred from CO or 2MASS maps. We refer the reader to Gómez de Castro et al. (2015) for a detailed discussion on this issue. Note that the *GALEX* survey is significantly shallower

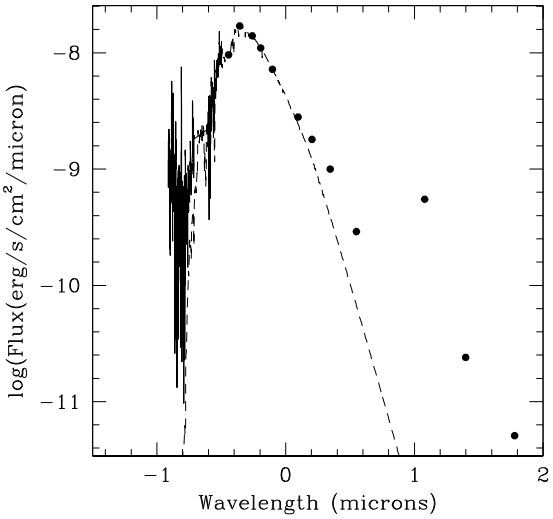

Figure 5. Spectral energy distribution of the CTTS binary AK Sco composed by two F5 stars. The *IUE* UV spectrum of AK Sco as well as the photometric data from Alencar et al. (2003) are represented. The Kurucz model of a F5 star is overlaid (dashed line).

than the 2MASS survey for galactic sources because extinction prevents UV radiation to propagate long distances in the galactic plane. Henceforth, no UV candidates to TTSs are lost in the cross-matching procedure.

3.1. Basic Selection Criteria for TTSs

Only 1% of sources, out of a grand total of 163,313 sources, are detected both in the NUV and FUV bands; they constitute our working sample since our goal is to search for bona fide candidates instead of guaranteeing that no TTS in the field is lost in the search. In practice, this means that some weak TTSs or brown dwarfs may not be included in the list, as they are too faint to be detected in the FUV band. However, even with this restrictive criterium, the known TTSs in the area mapped by *GALEX*/AIS are retrieved (see below), though some of them, like LkCa 1, lie very close to the sensitivity limit in the FUV band.

The (FUV-J, $J-K$) and (NUV-J, $J-K$) diagrams are plotted in Figure 7. Note that the colors of the vast majority of the sources agree with the predictions of the Kurucz models for main-sequence stars (compare Figure 7 with Figure 4 in FH). The location of the *IUE* qualification sample is clearly different from that of the dominant galactic population in the plot; the $J-K$ color of classical TTSs exceeds that of the field (main) sequence stars by more than 5σ according to FH's Figure 4.

At this point, it is worth noting the differences between the procedures used in FH and in this work to identify TTSs candidates. In this work, we define candidates by *TTS class membership*, while FH define their TTSs candidates by not belonging to the *main-sequence class membership*; this last one being defined from a sample of field stars. FH used field star

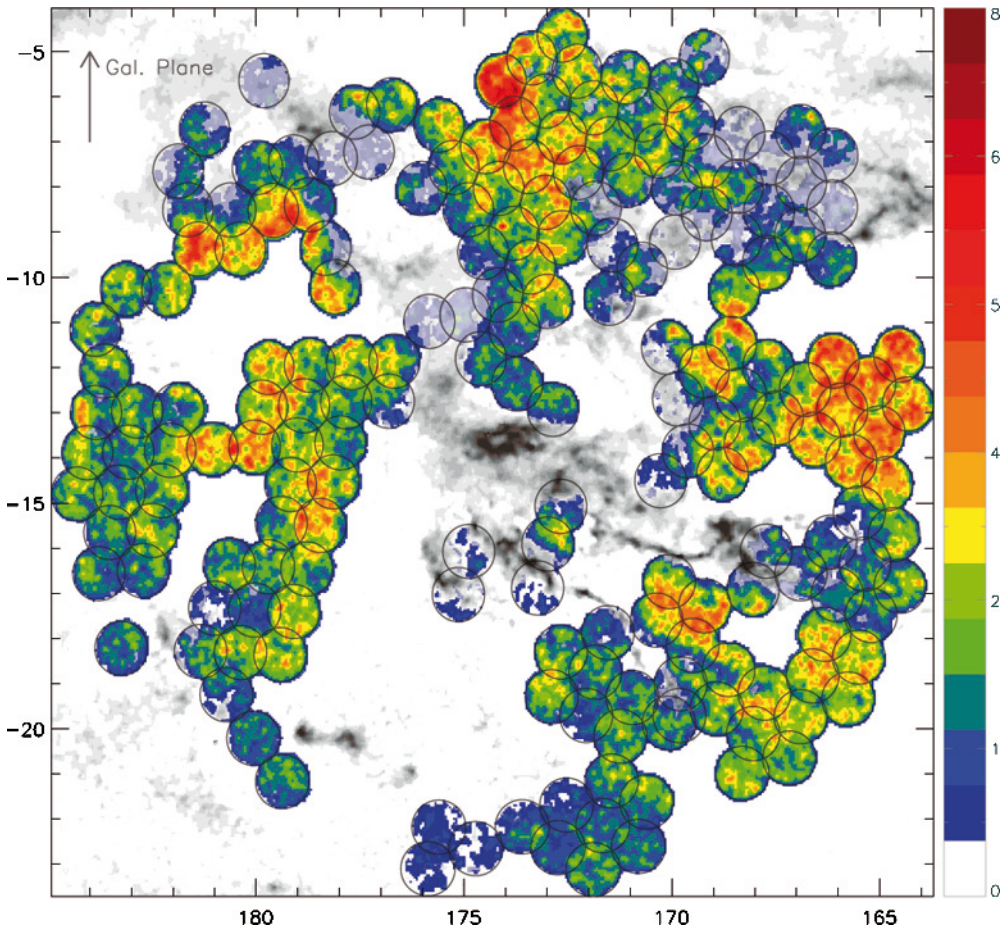

Figure 6. Density of NUV *GALEX* sources in the TMC. The densities are color coded in stars per 3 arcmin^2 (see lateral bar). The molecular gas distribution, as unveiled by the 2MASS extinction map (Lombardi et al. 2010) is overlaid for reference.

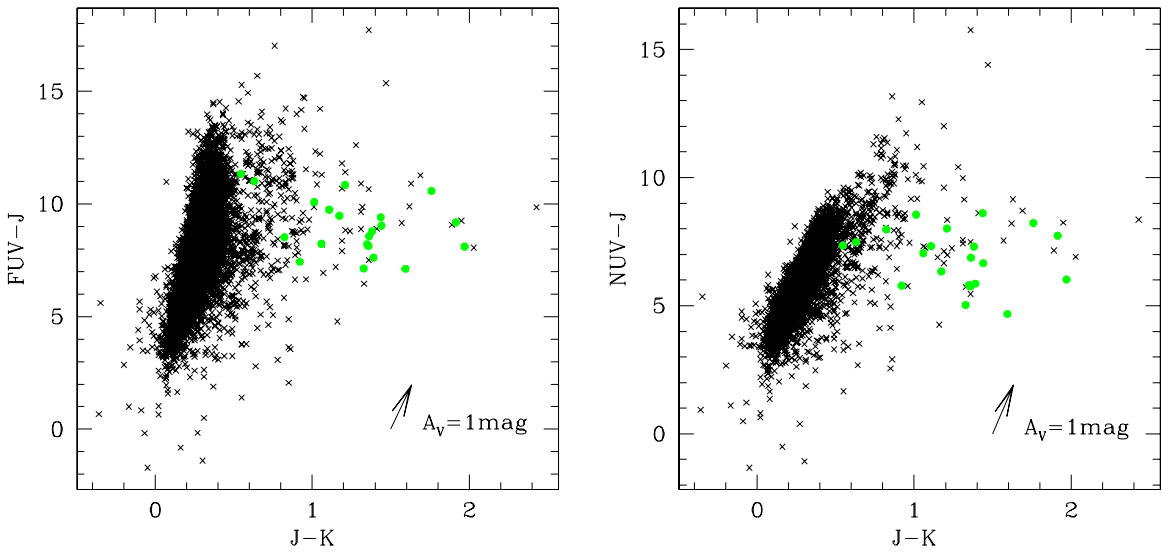

Figure 7. Color–color diagrams for the survey stars (black dots) and the *IUE* TTSs qualification sample (green circles) to be compared with Findeisen & Hillenbrand (2010) work.

photometry and an iterative procedure to define the locus of the main-sequence stars with a linear regression line in the (FUV-J) and (NUV-J) versus ($J-K$) diagram. However, we identify as candidates those sources that share the same color as the well-known TTSs of the *IUE* template sample; thus, no further assumptions are introduced. According to our criterium, TTSs candidates have to satisfy 7 mag < FUV − J <12 mag and 4 mag < NUV − J < 9 mag, however, some of FH's candidates lie outside these boundaries. The extinction arrows have been plotted using the coefficients derived by Yuan et al. (2013) for the Fitzpatrick extinction law. Note that the TTSs in the qualification sample have well-studied extinctions with $A_V = 0.1$–1.5 mag; the two WTTSs are very close to the field stars location.

At this point, it is worth remembering the main sources of extinction in the TTSs environment: the circumstellar (CS) and the interstellar medium (ISM). For TTSs in the TMC, ISM extinction is mainly caused by the molecular cloud; the complex is located at the outskirts of a low-density bubble in the local ISM (see, i.e., the Ungerechts & Thaddeus 1987 CO survey of the area). At early stages, TTSs can be deeply embedded in the cloud and totally occulted at UV or optical wavelengths; as indicated above, even a very bright TTS, such as RW Aur, would not be detected in the FUV band for $A_V = 2.7$ mag. For this reason, the *GALEX* survey has avoided dark molecular cores and only covers the halo where extinction is significantly low, $N_H < 8.8 \times 10^{20}$ cm^{-2} or $A_V < 0.5$ mag, as inferred by comparing Figure 5 with Lombardi et al. 2010 (see also Gómez de Castro et al. 2015). CS extinction is linked to the nature of TTSs (dusty disk atmospheres, orientation effects; see, i.e., Watson et al. 2007 or Dullemond et al. 2007) and, as such, it is used to qualify the candidates.

The generic feature characterizing TTSs is the coexistence of FUV, NUV, and infrared excess; this is also shown in Figure 8 where the optical B, V, and R bands are used as fiducial pivot bands for the photospheric radiation. Optical photometry has been retrieved after cross-correlation with UCAC4 for the candidate sources (see above).

The separation between TTSs and the galactic stellar population is clean, except for weak lined TTSs (WTTSs). Sources like AB Dor or HD 283572 (see Table 1) are located in the same region as the main-sequence stars in the color–color diagrams involving the NUV band.

In Figure 9, UV versus infrared colors are directly plotted. The UV color, FUV–NUV, is a mixed index that includes the following: (1) the excess of the hard UV radiation (C IV, Si IV, He II) over the soft UV radiation (Balmer continuum, Fe II, C II, Mg II), as well as (2) the excess radiation produced by the reprocessing of Lyman α photons in the disk (see, i.e., France et al. 2012) with respect to the photospheric and chromospheric radiation flux. This index is plotted against the $J-K$ and the H-K infrared colors. H-K is considered to be a good estimator of the accretion rate (see, i.e., Meyer et al. 1997 for details), however, WTTSs are not well discriminated from main-sequence stars in H-K. The $J-K$ color is a much more reliable tracer (see Figure 9). Therefore, we will consider the FUV–NUV versus $J-K$ diagram as our prime diagram for selecting TTSs candidates from the *GALEX* survey. Note that the impact of interstellar extinction on candidate selection is small in the color–color diagrams. Also, $A_V > 2$ mag to shift a given source from the field stars stripe into the TTSs locus within the diagram (see Section 3.3 for a discussion on WTTSs).

We have also considered other diagrams such as NUV-R versus $J-K$ and NUV-H versus $J-K$ to search for candidates. They are useful for characterizing the young stellar population in farther regions (such as Orion) where most of the TTSs are not detectable in the FUV band. A preliminary list of 315 TTSs candidates has been generated including all sources that satisfy at least one of the following criteria.

1. *Criterium I: FUV–NUV versus J-K*. TTSs satisfy 0.5 < $J - K$ < 2.4 and 0.4 < FUV − NUV < 4.6.
2. *Criterium II: FUV–NUV versus H-K*. TTSs satisfy 0.2 < $H - K$ < 1.2 and 0.4 < FUV − NUV < 4.6.
3. *Criterium III: NUV-R versus J-K*. TTSs satisfy 0.5 < $J - K$ < 2.4 and 1.5 < NUV − R < 8.2.
4. *Criterium IV: NUV-H versus J-K*. TTSs satisfy 0.5 < $J - K$ < 2.4 and 4.2 < NUV − H < 11.0.

This list has been purged of spurious sources using the services of the Stellar Data Base at the Centre de Données Stellaires in Strassbourgh (CDS). CDS provides information on the

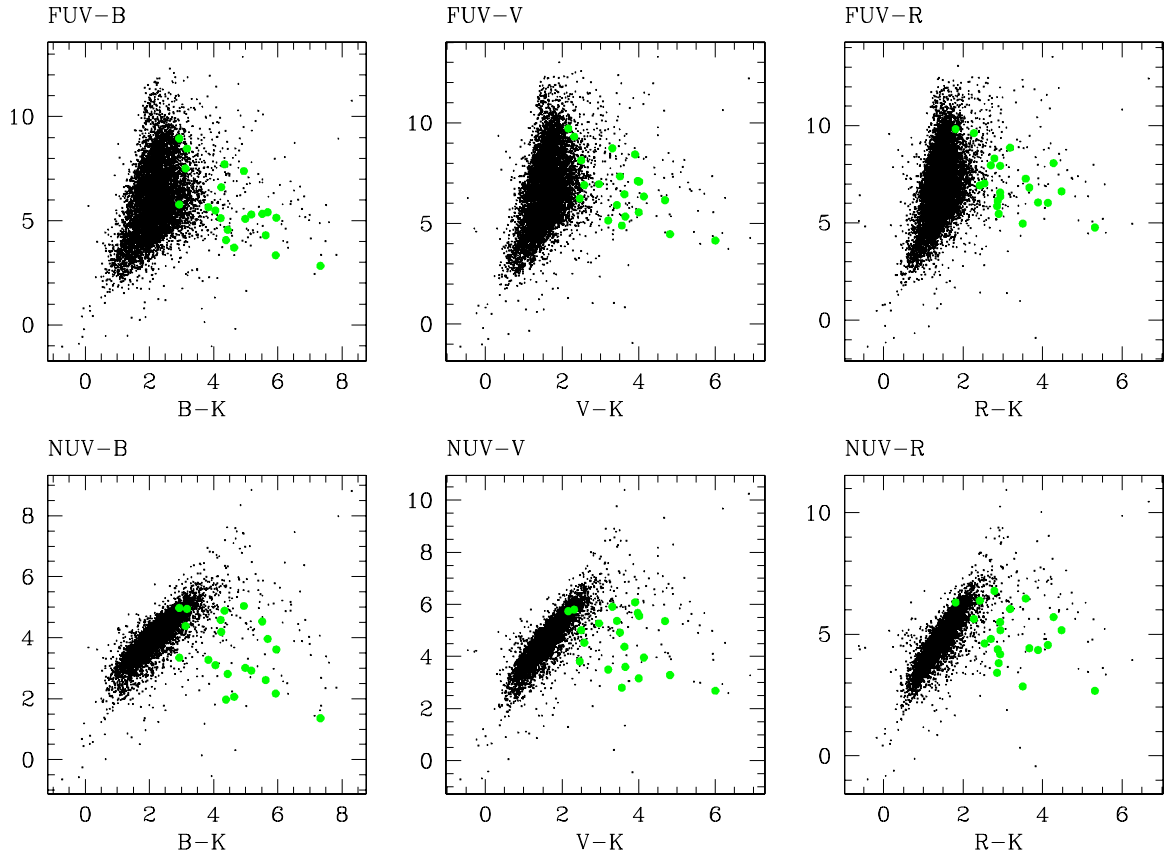

Figure 8. Color–color diagrams showing the UV and infrared excess with respect to the photosphere for the survey stars (black dots) and the *IUE* TTSs qualification sample (green circles).

object type[3] that is defined as a hierarchical classification, which emphasizes the physical nature of the object rather than peculiar emission in some region of the electromagnetic spectrum or the location in peculiar clusters or external galaxies. The two main channels for feeding the database are the daily scanning of papers published in the astronomical literature providing new references and new identifiers for existing objects, as well as the complete (or partial) folding of selected catalogs into the database, which serves as the basis for improving the completeness and multi-wavelength coverage of the database (see Wenger et al. 2000). Only objects classified as TT*, Em*, or without CDS identification are kept. The CDS bibliographic service has also been used to refine further the identification. Most of the stars classified as Em* are found to be WTTSs. Also, some TTS candidates from the WISE survey (Rebull et al. 2011) or from old *ROSAT*-based surveys (Wichmann et al. 1996, Li & Hu 1998) are recovered in our *GALEX*-based search for candidates.

The selection procedure is robust; all known CTTSs included in the fields mapped by the *GALEX*/AIS are recovered in this list of candidates. This includes the CTTSs HBC425, CI Tau, GH Tau,V807 Tau, ZZ Tau, DK Tau, IQ Tau, FP Tau, CX Tau, CW Tau, FM Tau, Elias 12, V773 Tau, V836 Tau, IRAS04108+2910, GM Aur, RW Aur, and UY Aur.

Both GM Aur and RW Aur were also part of the *IUE* qualification sample of TTSs. The discrepancy between their *GALEX* FUV and NUV magnitudes and those calculated from the *IUE* spectra is smaller than the typical variability range of CTTSs: < 0.75 mag or a factor of 2 in flux. The strongest discrepancy is found in the FUV magnitude; $\Delta\mathrm{FUV} = \mathrm{FUV}_{GALEX} - \mathrm{FUV}_{\mathrm{IUE}} =$ 0.5 mag for RW Aur but this can be easily accounted for by the large intrinsic variability of this source (see, e.g., Gómez de Castro & Verdugo 2003).

Well-known WTTSs are also retrieved with our search criteria, namely, HD30171, RXJ0437.4 + 1851B, V1207 Tau, V1195 Tau, LkCa 1, HD 281691, LkCa 19, V600 Aur, and V583 Aur. Our candidate list includes some WTTSs discovered recently from the analysis of the *Spitzer* data (IRAC) of the TTSs candidates identified in the WISE survey (Rebull et al. 2011), i.e., the binary BS Tau or 2MASSJ043601+1726120 (Esplin et al. 2014). However, they only satisfy our prime criterium (criterium I).

In summary, 31 out of the 315 candidates in the preliminary list are well-known TTSs. This extends the *IUE* working sample, especially in terms of WTTSs, permitting us to analyze the overall photometric properties of the TTSs as a class from the FUV to the IR (see Section 4).

3.2. UV Color–Magnitude Diagrams

UV color–magnitude diagrams are represented for the candidates in Figures 10 and 11. The depth of the *GALEX* survey is best visualized in Figure 10; the limiting FUV magnitude of 22.3 mag shows NUV $<$ 22.3 − [FUV − NUV] to be the limiting boundary. TTSs from the *IUE* sample have also been plotted; their NUV and FUV magnitudes have been corrected to the TMC distance (140 pc) for the figure. Extinction arrows are plotted for a 7,000 K spectrum (as in Yuan et al. 2013 for the Fitzpatrick extinction law) and for T Tau, both for $R = 3.1$. Note the sensitivity of the color correction to the underlying energy distribution.

[3] simbad.u-strasbg.fr/simbad/sim-display?data=otypes

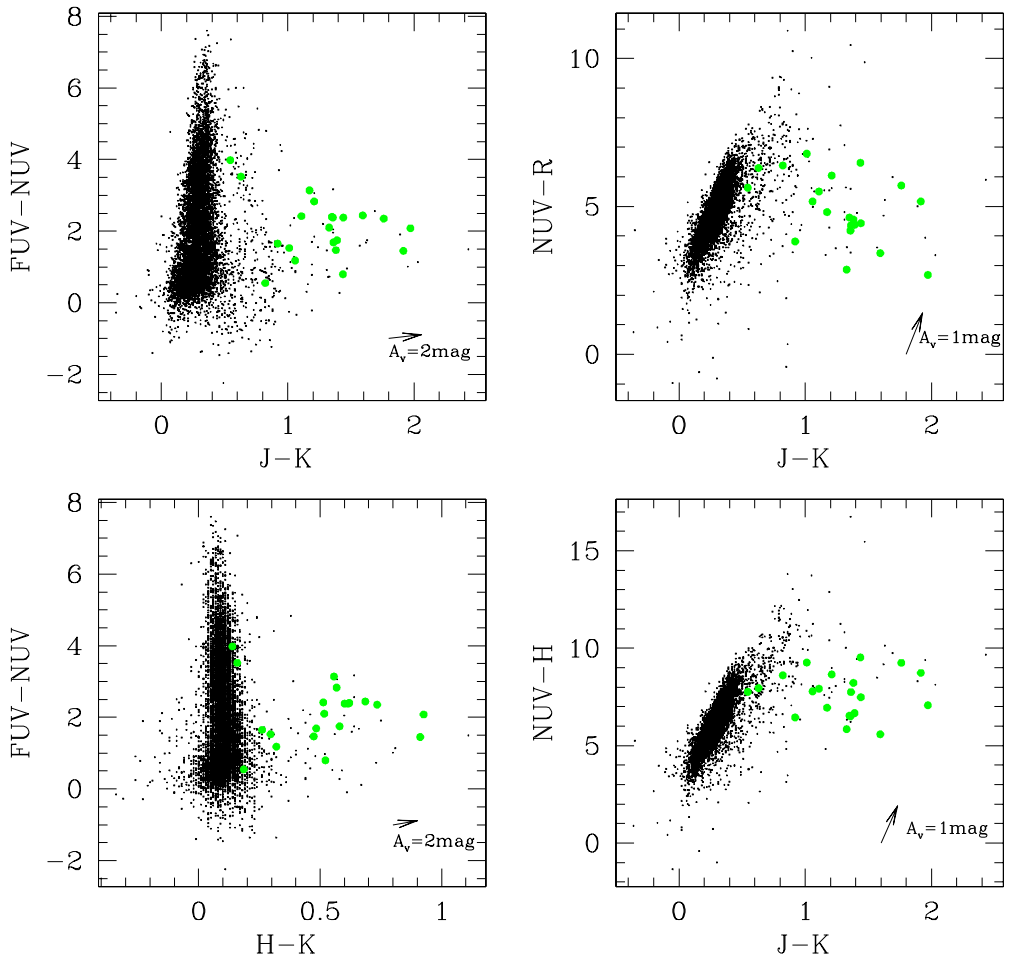

Figure 9. Color–color diagrams used to select candidates to TTSs in the *GALEX* fields. Survey stars and the *IUE* qualification sample are represented by black dots and green circles, respectively.

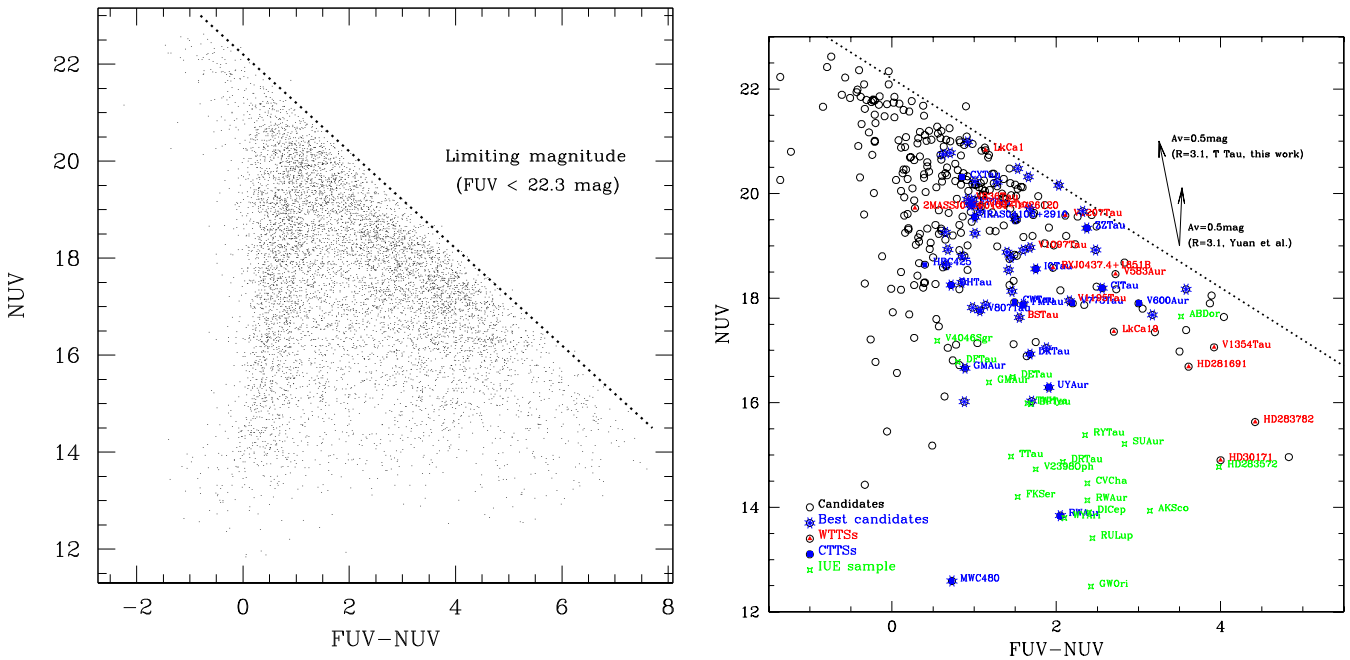

Figure 10. NUV vs. FUV–NUV color–magnitude diagram for the FUV sources in the *GALEX* AIS survey of the TMC. Left panel: all survey sources are represented. The limiting magnitude boundary is marked with a dashed line. Right panel: candidates found in this work and the *IUE* sample of TTSs are marked with open black circles and green stars, respectively. The magnitudes of the TTSs in the *IUE* sample have been set at a distance of 140 pc (the distance to the TMC) for reference. The candidates satisfying all the four criteria (see Section 3.1) are marked with blue asterisks. The known TTSs recovered in the search for candidates are indicated: CTTS (blue squares) and WTTS (red triangles). Extinction is marked from Yuan et al. 2013 (for the Fitzpatrick extinction law) and for T Tau, both for $R = 3.1$.

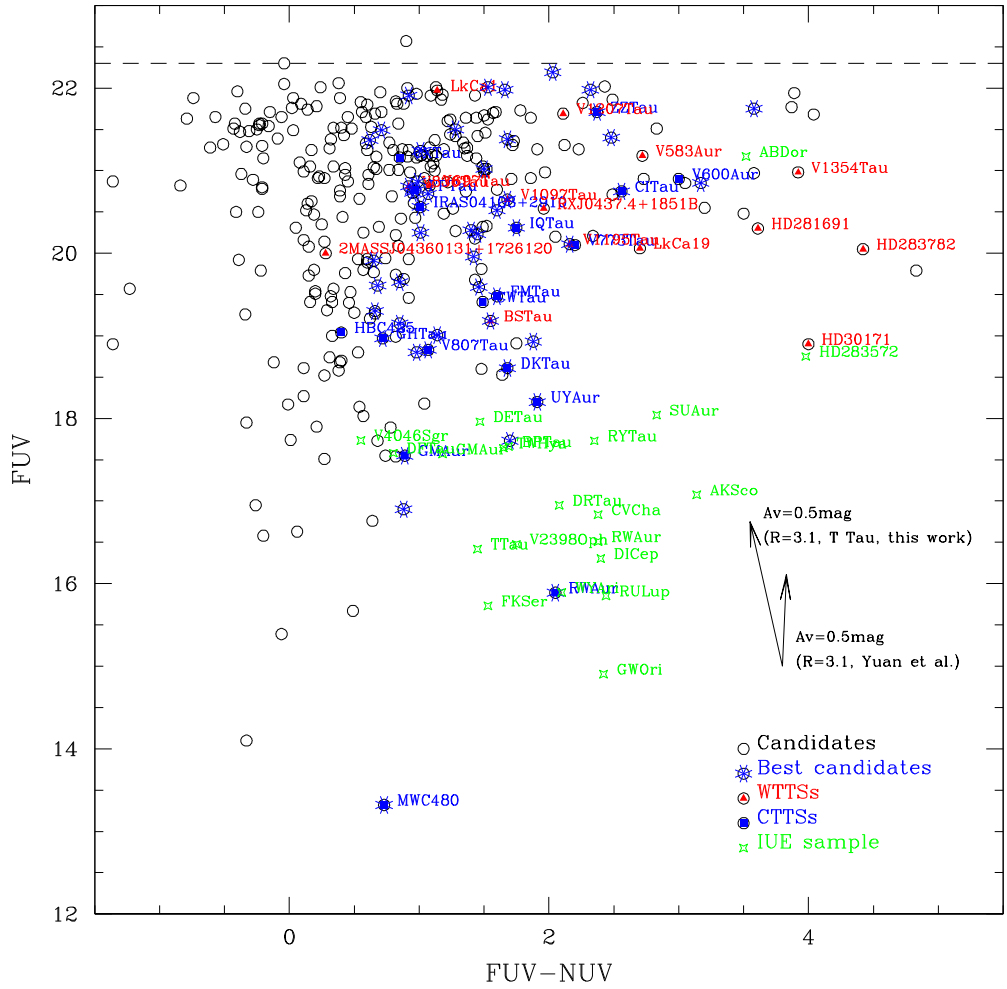

Figure 11. Same as Figure 10, but for the FUV vs. FUV–NUV color–magnitude diagram. The dashed line represents the FUV magnitude that the 2M1207 brown dwarf would have if located at the center of the Hyades open cluster (45 pc).

Let us first examine the NUV versus FUV–NUV diagram. The WTTSs are close to the sensitivity boundary and are the reddest sources in the plot. Also note that CTTSs are not only brighter but also significantly bluer than WTTSs. We have computed a statistic distribution function to this boundary for CTTSs and WTTSs to quantify this qualitative behavior. The WTTSs distribution has a single peak with $d_{\rm lim} = 1.31 \pm 0.65$ mag, however, CTTSs have a main peak at $d_{\rm lim} = 3.15$ mag and a broad tail to lower distances. This broad distribution is associated with the CTTSs spectral type, that is, M-type CTTSs are located closer to the limiting magnitude boundary than earlier types.

In the FUV versus FUV–NUV plot (Figure 11), there is not such a clear trend. Most of the candidates are close to the limiting magnitude boundary. It is worth noting that stars as active as AB Dor should be detectable at the distance of the TMC from the *GALEX*/AIS.

To obtain further insight into the low-luminosity limit, we have retrieved from the *HST* archive the ultraviolet spectrum of the only brown dwarf observed, 2MASS J12073346 39322539,[4] hereafter 2M1207. This is an M8 brown dwarf located in the TW Hya association at 52.4 pc (Webb et al. 1999). Unfortunately, the observation only covers the FUV *GALEX* band. The *GALEX*/AIS limiting magnitude in this band, 22.3, corresponds to a flux of 5.74×10^{-17} erg s^{-1} cm^{-2} Å^{-1} which is slightly higher than the integrated 2M1207 flux in the FUV band (4.01×10^{-17} erg s^{-1} cm^{-2} Å^{-1}); the 2M1207 FUV magnitude is 22.7. In summary, brown dwarfs similar to 2M1207 are very close to the *GALEX*/AIS detection limit if located at a distance comparable to the mean distance of the Hyades open cluster, 45 pc (de Bruijne et al. 2001), as shown in Figure 11.

Finally, note that the separation between CTTSs and WTTSs in Figure 10 is nearly vertical, similar to the extinction law. This shows that there is an extinction-accretion degeneracy; extinction makes the sources weaker while accretion produces an increase in the TTSs luminosity both producing mild signature in the FUV–NUV color.

3.3. Refining the Sample: Hot Star Removal

Two out of the four criteria indicated in Section 3.1 do not impose any constraint on the FUV–NUV color. As a result, the first list of candidates includes some hot sources with colors of FUV − NUV < 0.4. Some of these could just be hot stars in the field. In principle, we could remove them directly from the list of candidates, but we prefer to use a more sophisticated procedure that takes into account the SED (and not just one color), since we have detected some well-known TTSs, such as HBC 425 (with FUV − NUV > 0.4), that would be missed with

[4] The data set used was lb4p01010 and the observations were obtained with the Cosmic Origins Spectrograph and grating G140L in 2009 December 3 (see France et al. 2010).

a single color filter. Thus, we have decided for the SED fitting to make a simple determination of the effective temperature and remove from our list of candidates sources with $T_e > 7{,}500$.

We have built the optical SED for the whole set of candidates using UCAC4 photometry; the optical range is the best suited to estimate the stellar effective temperature for spectral types F-M. Afterward, we used the VOSA tool of the Virtual Observatory[5] to fit photospheric models to each candidate and determine its effective temperature.

VOSA combines the multiwavelength data from generic archives and catalogs within a VO environment to find the best fit to a predetermined set of theoretical models. The provided best fitting model is the one that minimizes the value of the reduced χ^2, defined as

$$\chi^2 = \frac{1}{N-P}\sum\left(\frac{1}{\sigma_0^2}(Y_0 - M_d Y_m)^2\right),$$

where Y_0 is the observed flux, σ_0 is the observational error in the flux, N is the number of photometric data points, P is the number of parameters being fitted, Y_m is the theoretical flux predicted by the model, and M_d is the multiplicative dilution factor, defined as $(R/D)^2$ (for models from Hauschildt et al. 1999; Allard et al. 2011 and Chabrier et al. 2000), with R being the radius of the source and D the distance to the object (we refer the reader to Bayo et al. 2008 for a more detailed description of the method and the goodness of the estimates). Stellar models implemented in VOSA are the Kurucz, NextGen, or DUSTY00 stellar models. The DUSTY00 synthetic models account properly for the effect of dust grain formation in the atmosphere of very cool stars and brown dwarfs. NextGen models represent a later elaboration in the synthetic spectra of cool stars (see Allard et al. 2012, for further details).

As its standard output, VOSA produces several parameters, including effective temperature. Taking into account the small number of data points available per star, we worked with a reduced set of free parameters, fixing metallicity to solar and extinction to 0 mag. Note that extinction causes the SED to become redder and thus cooler. As a result, reddened hot stars may be kept in the sample but those sources with high T are certainly not TTSs since the UV excess of the TTSs is not high enough to mimic early spectral types (see Figure 5).

After rejection of sources with effective temperatures above 7500 K, our list of candidates was reduced to 212 sources.

4. PHOTOMETRIC PROPERTIES OF THE TTSs FROM FUV TO IR: FURTHER REFINEMENT OF THE TTSs CANDIDATES LIST

As pointed out in Section 3, the detection of known TTSs in the TMC has significantly increased the photometric database of TTSs in the *GALEX* bands from our primitive *IUE* sample, especially concerning WTTSs. The new sample includes 15 WTTSs and 31 CTTSs, 10 of which are M-type stars providing better statistics for the candidates search. As shown in Figure 12, the best diagram to discriminate TTSs from the galactic field stellar population remains the FUV–NUV versus $J-K$ diagram. However, new trends can now be identified, such as the following:

1. the locus of the WTTSs is well defined by the line $\mathrm{FUV}-\mathrm{NUV} = (-3.88 \pm 0.61)(J-K) + (5.64 \pm 0.55)$, with RMS = 0.59. The dispersion of WTTSs around this linear regression line has been computed and used to define the 3σ boundary marked with dashed lines in Figure 12;
2. the locus of the CTTSs in $J-K$ is well defined by a normal distribution centered at $(J-K) = 1.4$ with dispersion $\sigma = 0.4$. However, in FUV–NUV, the only constraint set by the data is $0 < \mathrm{FUV}-\mathrm{NUV} < 3.5$, which is very similar to our criteria in Section 3.

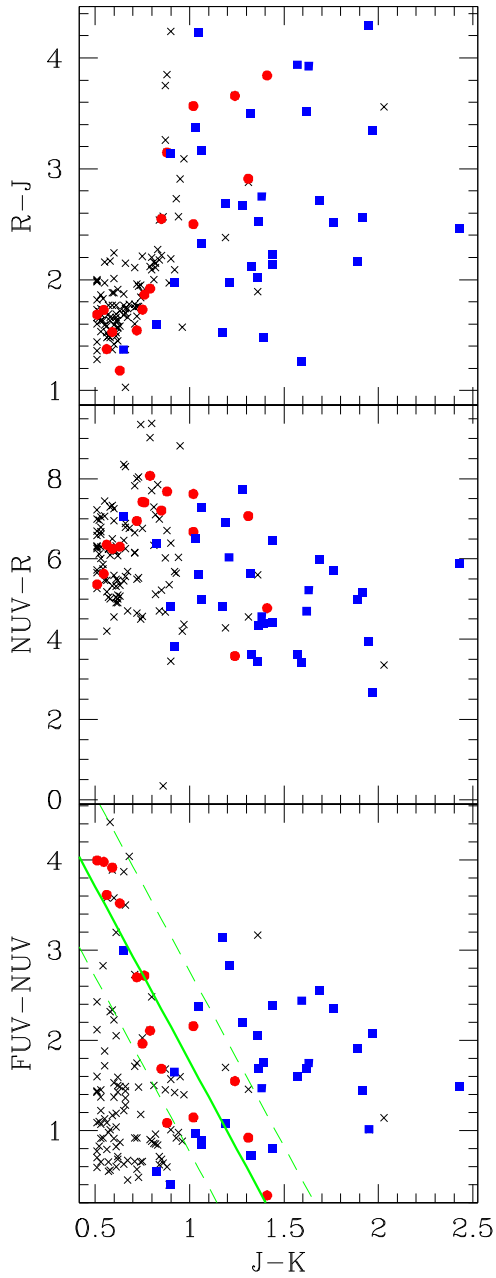

Figure 12. Color–color diagrams for the final selection of TTSs candidates. Candidates are marked with black crosses, and CTTSs and WTTSs from the qualification sample are represented by blue squares and red circles, respectively. The regression line of the WTTSs in the FUV–NUV vs. $J-K$ diagram is plotted (solid line).

These constraints have been used to reduce the list of 212 candidates (see Section 3) to just 63 (see Table 2) by basically removing from the list of candidates those stars with small $J-K$ and FUV–NUV colors. Note that there is some degree of overlap between WTTSs and CTTSs that corresponds to hot WTTSs with low infrared excess and CTTSs with small infrared excess,

[5] svo2.cab.inta-csic.es/theory/vosa/

Table 2
Extract of the Table with the TTSs and Candidates found in the TMC from the *GALEX* AIS

RA (deg)	DEC (deg)	FUV (mag)	NUV (mag)	R2 (mag)	*J* (mag)	*H* (mag)	*K* (mag)	ID	Obj. Type
60.18	28.87	20.21	17.87	12.54	11.17	10.66	10.58		Candidate
61.04	29.34	21.77	17.9	11.44	9.57	9.05	8.92		Candidate WTTS
61.5	29.94	20.85	17.68	12.08	10.19	9.47	8.83		Candidate CTTS
61.71	25.69	20.11	17.95	11.27	8.77	8.03	7.75	V1195Tau	WTTS
62.06	21.63	21.81	20.93	11.55	9.46	8.84	8.66		Candidate
62.06	30.26	21.37	20.75	16.04	13.86	13.31	13.02		Candidate
62.27	28.92	21.75	18.17	11.97	9.96	9.57	9.36		Candidate WTTS
62.29	29.02	20.3	16.69	10.33	8.96	8.51	8.4	HD281691	Candidate WTTS[a]

Note. [a] Also candidate to TTSs from the proper motions survey by Ducourant et al. (2005).
(This table is available in its entirety in machine-readable form.)

i.e., type II-III TTSs according to the standard infrared SED classification (Wilking & Lada 1983).

Using the constrains summarized above, the candidates have been classified in Table 2 as*candidates to WTTS*, *candidates to CTTS*, or just *candidates* depending on their location in the FUV–NUV versus $J-K$ diagram. WTTSs candidates are stars within 3σ of the WTTSs regression line that satisfy $\mathrm{FUV}-\mathrm{NUV} > 3.5$ to ensure that they are not in the area where the WTTSs and the CTTSs overlap in the diagram. CTTSs candidates are stars satisfying $0 < \mathrm{FUV}-\mathrm{NUV} < 3.5$ and lying outside the 3σ boundary around the WTTSs regression line. The rest of the sources have just been classified as TTS candidates.

Note that both WTTSs and CTTSs cover a broad range in FUV–NUV. In WTTSs, the FUV–NUV excess correlates well with the $J-K$ excess, but this is not the case for CTTSs. These stars are surrounded by accretion disks that are luminous in the infrared bands, breaking the expected correlation between the UV and infrared excess associated with the stellar spectral type. In an accretion-dominated SED, the correlation between the UV and IR excess should have a different functional form than observed in stars; moreover, inclination effects and extinction affect, in a different way, the disk radiation and the UV radiation from the accretion shocks and the stellar magnetosphere. CTTSs with similar accretion rates/luminosities and $J-K$ color may show small or high FUV–NUV values depending on whether the disk is seen face-on or pole-on, respectively (see, i.e., the determination of the disk inclination in the so-called silhouette disks; O'Dell et al. 1993). In fact, the uncorrelated combination of all of these effects is the most likely cause of the spreading observed in Figure 12.

5. DISCUSSION

The distribution of UV TTSs and candidates on the TMC is displayed in Figure 13; the previously known CTTSs and WTTSs are labeled. The new sources are concentrated in the filaments around $l \simeq 170°$–$174°$ and $b \simeq -4°$–$10°$ between the Auriga and the California complexes. Note that there is not a correlation between the spatial density of UV sources and TTS candidates (compare Figure 5 with Figure 13). The proper motions of the PMS stars in the region from Ducourant et al. (2005) are overlaid in Figure 13 for reference. They indicate the average direction of the TMC motion in the plane of the sky. As pointed out by Gomez de Castro & Pudritz 1992, the good kinematical coupling between the TTSs and the molecular cloud in radial velocity can be extrapolated to the filament kinematics in the plane of the sky.

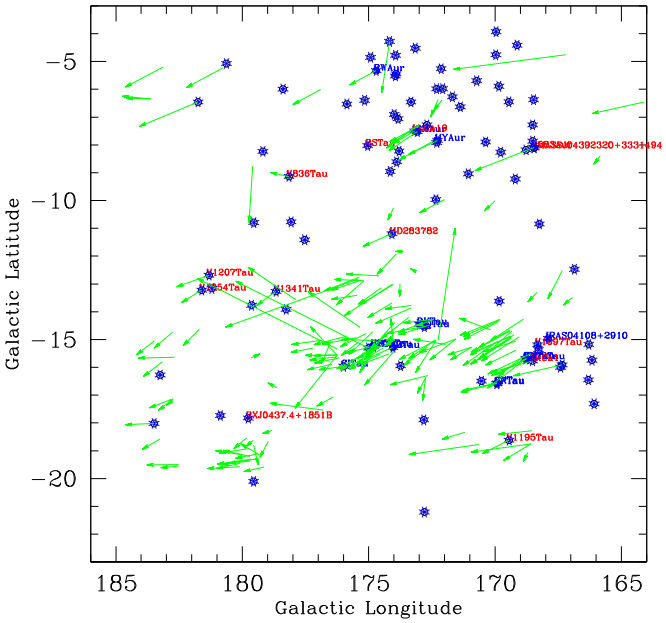

Figure 13. Location of the TTSs candidates over the TMC. The proper motions of the PMS stars in the TMC are also indicated (from Ducourant et al. 2005). The name of the known TTSs are indicated in red for WTTSs and in blue for CTTSs.

A global scenario was proposed by Gomez de Castro & Pudritz (1992) for star formation in Taurus. According to their scenario, the driving energy source of the cloud's hydromagnetic turbulence is the cascading of a large magnetic wave unveiled by the polarization maps of the region (Moneti et al. 1984). Recent evidence of hydromagnetic wave action in the Taurus filaments was found by Heyer & Brunt (2012) from the analysis of the CO data in Davis et al. (2010). According to this global scenario, the youngest sources should be at the cloud front where the molecular gas is concentrated. The most evolved TTSs are thus expected to be located at the rear of the cloud where most of the new candidate TTSs unveiled by this work have been found.

6. CONCLUSIONS

From an initial sample of about 350,000 UV sources in the TMC according to the *GALEX*/AIS catalog, a list of 63 bona fide candidates to TTSs has been produced. For this purpose, a first set of selection criteria have been defined based on the UV photometric properties of the TTSs to create an initial set of 315 candidates to TTSs; the SIMBAD service has been used to guarantee that only stellar unknown sources or known sources

classified as TTSs or Emission line stars are included. We have validated the procedure by recovering the 31 known TTSs in the area of the survey.

As an additional result, we have generated a list containing 15 WTTSs and 31 CTTSs that can be used as a qualification sample for UV-IR searches of TTSs in star forming regions. This qualification sample has been used to statistically improve the candidate selection criteria producing the final list of 63 bona fide TTSs candidates.

This research was partially supported by grant AYA2011-29754-C03-01 from the Government of Spain.

Facilities: GALEX, IUE, SIMBAD, 2MASS, VO, UCAC4, WISE.

REFERENCES

Alencar, S. H. P., Melo, C. H. F., Dullemond, C. P., et al. 2003, A&A, 409, 1037
Allard, F., Homeier, D., & Freytag, B. 2011, in ASP Conf. Ser. 448, 16th Cambridge Workshop on Cool Stars, Stellar Systems, and the Sun, ed. C. M. Johns-Krull, M. K. Browning, & A. A. West (San Francisco, CA: ASP), 91
Allard, F., Homeier, D., Freytag, B., & Sharp, C. M. 2012, in EAS Publication Ser., Vol. 57, Low-mass Stars and the Transition Stars/Brown Dwarfs, ed. C. Reylé, C. Charbonnel, & M. Schultheis (Cambridge: Cambridge Univ. Press), 3
Ardila, D. R., Herczeg, G. J., Gregory, S. G., et al. 2013, ApJS, 207, 1
Basri, G., & Batalha, C. 1990, ApJ, 363, 654
Bayo, A., Rodrigo, C., Barrado Y Navascués, D., et al. 2008, A&A, 492, 277
Bianchi, L., Conti, A., & Shiao, B. 2014, AdSpR, 53, 900
Bianchi, L., Herald, J., Efremova, B., et al. 2011, Ap&SS, 335, 161
Calvet, N., & Gullbring, E. 1998, ApJ, 509, 802
Chabrier, G., Baraffe, I., Allard, F., & Hauschildt, P. 2000, ApJ, 542, 464
Davis, C. J., Chrysostomou, A., Hatchell, J., et al. 2010, MNRAS, 405, 759
de Bruijne, J. H. J., Hoogerwerf, R., & de Zeeuw, P. T. 2001, A&A, 367, 111
Ducourant, C., Teixeira, R., Périé, J. P., et al. 2005, A&A, 438, 769
Dullemond, C. P., Hollenbach, D., Kamp, I., & D'Alessio, P. 2007, in Protostars and Planets V, ed. B. Reipurth, D. Jewitt, & K. Keil (Tucson, AZ: Univ. Arizona Press), 555
Esplin, T. L., Luhman, K. L., & Mamajek, E. E. 2014, ApJ, 784, 126
Feigelson, E. D., Getman, K., Townsley, L., et al. 2005, ApJS, 160, 379
Findeisen, K., & Hillenbrand, L. 2010, AJ, 139, 1338
Findeisen, K., Hillenbrand, L., & Soderblom, D. 2011, AJ, 142, 23
Fitzpatrick, E. L. 1999, PASP, 111, 63
France, K., Linsky, J. L., Brown, A., Froning, C. S., & Béland, S. 2010, ApJ, 715, 596
France, K., Schindhelm, E., Herczeg, G. J., et al. 2012, ApJ, 756, 171
France, K., Yang, H., & Linsky, J. L. 2011, ApJ, 729, 7
Furlan, E., Luhman, K. L., Espaillat, C., et al. 2011, ApJS, 195, 3
Gomez de Castro, A. I. 1997, A&A, 323, 541
Gómez de Castro, A. I. 2009, ApJL, 698, L108
Gómez de Castro, A. I. 2013a, in Planets, Stars and Stellar Systems. Vol. 4: Stellar Structure and Evolution, ed. T. D. Oswalt & M. A. Barstow (Dordrecht: Springer), 279
Gómez de Castro, A. I. 2013b, ApJ, 775, 131
Gómez de Castro, A. I., & Franqueira, M. 1997, ApJ, 482, 465
Gómez de Castro, A. I., Lopez-Santiago, J., Lopez-Martinez, F., et al. 2015, MNRAS, submitted
Gómez de Castro, A. I., Lopez-Santiago, J., Sestito, P., et al. 2011, Ap&SS, 335, 97
Gómez de Castro, A. I., & Marcos-Arenal, P. 2012, ApJ, 749, 190
Gomez de Castro, A., & Pudritz, R. E. 1992, ApJ, 395, 501
Gómez de Castro, A. I., & Verdugo, E. 2003, ApJ, 597, 443
Hauschildt, P. H., Allard, F., & Baron, E. 1999, ApJ, 512, 377
Herbig, G. H., & Bell, K. R. 1988, LicOB, 1111, 90
Herczeg, G. J., Linsky, J. L., Valenti, J. A., Johns-Krull, C. M., & Wood, B. E. 2002, ApJ, 572, 310
Heyer, M. H., & Brunt, C. M. 2012, MNRAS, 420, 1562
Hutchinson, M. G., Evans, A., Winkler, H., & Spencer Jones, J. 1990, A&A, 234, 230
Ingleby, L., Calvet, N., Herczeg, G., et al. 2013, ApJ, 767, 112
Jensen, E. L. N., Cohen, D. H., & Gagné, M. 2009, ApJ, 703, 252
Kenyon, S. J., Gómez, M., & Whitney, B. 2008, in Handbook of Star Forming Regions, Vol. 1: The Northern Sky, ed. B. Reipurth (San Francisco, CA: ASP), 405
Kohoutek, L., & Wehmeyer, R. 1999, A&AS, 134, 255
Lada, C. J. 1983, RMxAA, 7, 231
Lamzin, S. A. 1998, ARep, 42, 322
Lépine, S., & Gaidos, E. 2011, AJ, 142, 138
Li, J. Z., & Hu, J. Y. 1998, A&AS, 132, 173
Lombardi, M., Lada, C. J., & Alves, J. 2010, A&A, 512, AA67
Mendoza, V., & Eugenio, E. 1968, ApJ, 151, 977
Meyer, M. R., Calvet, N., & Hillenbrand, L. A. 1997, AJ, 114, 288
Moneti, A., Pipher, J. L., Helfer, H. L., McMillan, R. S., & Perry, M. L. 1984, ApJ, 282, 508
Montmerle, T., Koch-Miramond, L., Falgarone, E., & Grindlay, J. E. 1983, ApJ, 269, 182
Morrissey, P., Conrow, T., Barlow, T. A., et al. 2007, ApJS, 173, 682
Neuhaeuser, R., Sterzik, M. F., Schmitt, J. H. M. M., Wichmann, R., & Krautter, J. 1995, A&A, 295, L5
O'dell, C. R., Wen, Z., & Hu, X. 1993, ApJ, 410, 696
Padgett, D. L., Cieza, L., Stapelfeldt, K. R., et al. 2006, ApJ, 645, 1283
Preibisch, T. 2004, Ap&SS, 292, 631
Rebull, L. M., Koenig, X. P., Padgett, D. L., et al. 2011, ApJS, 196, 4
Siess, L., Dufour, E., & Forestini, M. 2000, A&A, 358, 593
Skrutskie, M. F., Cutri, R. M., Stiening, R., et al. 2006, AJ, 131, 1163
Strom, K. M., Strom, S. E., & Vrba, F. J. 1976, AJ, 81, 308
Takita, S., Kataza, H., Kitamura, Y., et al. 2010, A&A, 519, AA83
Ungerechts, H., & Thaddeus, P. 1987, ApJS, 63, 645
Valenti, J. A., Johns-Krull, C. M., & Linsky, J. L. 2000, ApJS, 129, 399
Watson, A. M., Stapelfeldt, K. R., Wood, K., & Ménard, F. 2007, in Protostars and Planets V, ed. B. Reipurth, D. Jewitt, & K. Keil (Tucson, AZ: Univ. Arizona Press), 523
Webb, R. A., Zuckerman, B., Platais, I., et al. 1999, ApJL, 512, L63
Wenger, M., Ochsenbein, F., Egret, D., et al. 2000, A&AS, 143, 9
Wichmann, R., Krautter, J., Schmitt, J. H. M. M., et al. 1996, A&A, 312, 439
Wilking, B. A., & Lada, C. J. 1983, ApJ, 274, 698
Yang, H., Herczeg, G. J., Linsky, J. L., et al. 2012, ApJ, 744, 121
Yuan, H. B., Liu, X. W., & Xiang, M. S. 2013, MNRAS, 430, 2188
Zacharias, N., Finch, C. T., Girard, T. M., et al. 2013, AJ, 145, 44